Spectrochimica Acta Part A: Molecular and Biomolecular Spectroscopy 348 (2026) 127158

Contents lists available at ScienceDirect

Spectrochimica Acta Part A:
Molecular and Biomolecular Spectroscopy

journal homepage: www.journals.elsevier.com/spectrochimica-acta-part-a-molecular-and-biomolecular-spectroscopy

New concept of spectroscopic detection of the cationic porphyrin via its spontaneous aggregation at Au@thermoresponsive polymer core@shell nanocomposites

Karolína Šišková [a,*], Nekane Guarrotxena [b], Miriam Guadano Sanchez [b], Josef Kapitán [c]

[a] Dept. of Experimental Physics, Faculty of Science, Palacký University Olomouc, 17. Listopadu 12, 771 46 Olomouc, Czech Republic
[b] Nanohybrid and Interactive Polymers Group, Institute of Polymer Science and Technology, Spanish National Research Council (ICTP-CSIC), Juan de la Cierva, 3, E-28006 Madrid, Spain
[c] Dept. of Optics, Faculty of Science, Palacký University Olomouc, 17. Listopadu 12, 771 46 Olomouc, Czech Republic

HIGHLIGHTS

- Generation of cationic porphyrin J-aggregates on Au@polymer nanocomposite surface.
- Positively charged model adsorbate getting concentrated at nanocomposite.
- Improved spectroscopic detection due to the thermoresponsiveness of polymeric shell.
- Two-step aggregation of the tetracationic porphyrin.
- Detection of therapeutically-active species at their relevant concentrations.

GRAPHICAL ABSTRACT

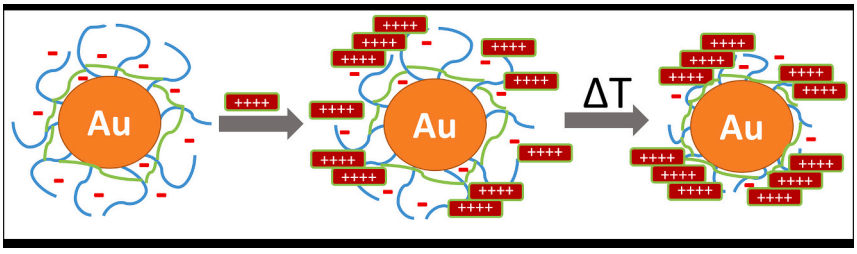

ARTICLE INFO

Keywords:
Smart polymer
Gold nanoparticle
Nanoparticle surface coating
J-aggregates
Substituted porphine macrocycle
TMPyP spectral form

ABSTRACT

Spectroscopic detection represents a big part of biomedical, biological, material, and environmental research. Here, the formation of J-aggregates of a tetra-cationic porphyrin (TMPyP), serving as a model adsorbate and known as a sensitizing part of antitumor and therapeutically-active agents, has been evidenced by several spectroscopic methods such as: UV–vis absorption spectroscopy, steady-state fluorescence, resonance Raman scattering (RRS) and surface-enhanced resonance Raman scattering (SERRS). It should be noticed that the tetra-cationic porphyrin does not form aggregates at low concentrations in water spontaneously, nor in the presence of low-molecular-weight species enveloping Au nanoparticles (AuNPs, prepared as references by citrate- and/or borohydride-induced reductions); indeed, rather an aggregation of AuNPs with adsorbed TMPyP were observed in these systems. On the contrary, at the surface of core@shell nanocomposites containing plasmonic AuNPs as a

Abbreviations: Au20PM, nanocomposite consisting of gold nanoparticles (20 nm in diameter) surrounded by a shell of poly-2-(2-methoxy-ethoxy)ethyl- methacrylate; Au60PM, nanocomposite consisting of gold nanoparticles (60 nm in diameter) surrounded by a shell of poly-2-(2-methoxy-ethoxy)ethyl- methacrylate; Au100PM, nanocomposite consisting of gold nanoparticles (100 nm in diameter) surrounded by a shell of poly-2-(2-methoxy-ethoxy)ethyl- methacrylate; Au60PN, nanocomposite consisting of gold nanoparticles (60 nm in diameter) surrounded by a shell of poly-N-isopropyl-acrylamide; Au60PS, nanocomposite consisting of gold nanoparticles (60 nm in diameter) surrounded by a shell of polystyrene, AuNPs = gold nanoparticles; MLSCC, monolayer surface-coverage concentration; NPs, nanoparticles, PDT = photodynamic therapy; RS, Raman scattering; RRS, resonance Raman scattering; SERS, surface-enhanced Raman scattering; SERRS, surface-enhanced resonance Raman scattering; TMPyP, 5,10,15,20-tetra-(*N*-methyl-4-pyridyl)porphyrin; MPyP6, TMPyP in 1 μM final concentration; TMPyP7, TMPyP in 0.1 μM final concentration..

* Corresponding author.
E-mail address: karolina.siskova@upol.cz (K. Šišková).

https://doi.org/10.1016/j.saa.2025.127158
Received 9 April 2024; Received in revised form 15 July 2024; Accepted 6 November 2025
Available online 7 November 2025

core (of three different sizes: 20, 60, and 100 nm) and selected polymers (two thermoresponsive polymers: poly-N-isopropyl-acrylamide and poly-2-(2-methoxy-ethoxy)ethyl-methacrylate, and polystyrene as a reference) as a shell, J-aggregates of TMPyP were detected by UV–vis absorption, fluorescence, RRS and SERRS for the first time in the present work. The mechanism of spontaneous J-aggregates formation of TMPyP at the nanocomposite surface (in TMPyP concentrations falling well below and/or being slightly above monolayer surface-coverage values) is suggested based on (i) coulombic attraction and (ii) amphiphilicity of the polymeric shells. Slightly elevated temperature (32 °C) and prolonged time of ageing (1 month) of the AuNPs@thermoresponsive polymer nanocomposites with adsorbed porphyrin resulted in a further increase of TMPyP J-aggregates formation. This can be regarded as the second aggregation step of the tetra-cationic porphyrin molecules stuck into polymeric shells that is beneficial for its spectroscopic detection. It can be envisaged that the concept of concentrate formation (aggregation) and spectroscopic detection of low concentrations of any species (even extremely charged and well dissolved in aqueous solution) via its spontaneous aggregation at the surface of AuNPs@thermoresponsive polymer core@shell nanocomposites, more pronounced at slightly elevated temperatures, and concomitant aggregation-induced fluorescence quenching of fluorophores could be exploited in biomedical, biological, material, and environmental research domains.

1. Introduction

Optical spectroscopies, such as UV–visible (UV–vis) absorption, fluorescence, Raman scattering (RS) and surface-enhanced Raman scattering (SERS) are substantial techniques of species detection in aqueous media due to negligible interference of water signal (which is contrary to infrared absorption spectroscopy for instance). UV–vis spectrophotometers are common in laboratories and generally used by scientists as a basic characterization and detection method, while fluorescence, RS and SERS are available rather in spectroscopically oriented laboratories. Fluorescence and SERS enable highly sensitive and very selective detection with high enhancement factors, respectively [1]. Recently, fluorescence has been employed in rapid, sensitive, on-site detection of species (e.g. [2]), and SERS in label-free detection and real-time in vivo monitoring of biologically important molecules and/or pollutants of emerging concerns (e.g. [3–6]). It should be noted that fluorescence is characteristic by a rather broad band, whereas RS/SERS manifests itself by well-resolved patterns which reflect and are very sensitive to any changes within the vibrational state of the molecule under study. Thus, RS/SERS spectra give more detailed structural information about the studied molecule than fluorescence.

Usually, noble metal (Au, Ag) nanoparticles (NPs) of various sizes and shapes and/or their dimers are exploited in the optical signal enhancement of species located in the near vicinity of the NPs surface [7,8]. Besides dimers, sharpened morphologies and/or intergrown noble metal NP aggregates are generated to create “hotspots” with large electromagnetic field enhancements [9–11]. In SERS-active systems exploiting hotspot formation, NPs aggregation leading to SERS signal increase is employed frequently. This working strategy is inverted in the present work: adsorbate molecules are aggregated instead of AuNPs. The advantage is that the aggregation of any organic species leads to their increased concentration at the close vicinity of the NP surface. Moreover, in the case of organic fluorophores, aggregation induces their fluorescence quenching [12]. This is again beneficial for SERS measurements because troubles with broad fluorescent backgrounds can be solved simultaneously. Hence, there are two independent spectroscopic methods, fluorescence and SERS, each based on a different principle, confirming the formation of adsorbate aggregates. The former spectroscopic method should provide a decreasing trend of signal, while the latter an increasing one when adsorbate aggregation occurs.

Aggregation of noble metal NPs can be suppressed either electrostatically, sterically, or owing to a combination of both manners [13]. On the other hand, adsorbate aggregation at noble metal NPs can be achieved by noncovalent interactions of adsorbate molecules with specifically designed NP surfaces and/or by balancing electrostatic charges of the adsorbate. Therefore, by tailoring a protecting layer (a shell) around the plasmonic NP core, both requirements can be efficiently fulfilled (i.e., adsorbate aggregation is pronounced, whereas NPs aggregation suppressed). There may be low-molecular weight and/or polymeric compounds employed as the protective shell around NPs.

Recently, stimuli-responsive polymers, as a new category of smart materials, have been used in water treatment via a stimuli-induced purification process and subsequent regeneration of the polymers, solving thus the sustainability issue concomitantly (e. g. [14]). Furthermore, plasmonic gold substrates grafted with a stimuli-responsive polymer [15] and/or hydrogel microspheres consisting of the same stimuli-responsive polymer, but decorated with Au nanorods [16] were successfully used in the detection of a model dye and/or an illegal pesticide, respectively. Inspired by these studies and based on our previous experience with stimuli-responsive polymers enabling the fine-tuning of noble metal NPs optical properties [17–22], we selected two thermoresponsive polymers, poly-N-isopropyl-acrylamide (pNIPAM), poly-2-(2-methoxy-ethoxy)ethyl-methacrylate ($pMEO_2MA$), and for comparison, a non-thermoresponsive polymer, polystyrene (pSTYRENE) for the present work. Contrary to the two above mentioned strategies (plasmonic substrates grafted with a stimuli-responsive polymer and polymeric microspheres decorated with Au nanorods), the thermoresponsive polymers create the protecting shell around AuNPs and hinder thus the direct contact of the selected adsorbate with AuNP surface in our present work; whereas polystyrene, serving as a reference, is rather eccentrically grown on AuNPs (forming thus a Janus type of NPs) to preserve the solubility of the resulting nanocomposite. In principle, the RS/SERS signal of the selected adsorbate could be even improved at elevated temperatures in the case of stimuli-responsive polymers, where the shell thickness varies according to the external stimulus (here temperature).

For the demonstration of the proposed concept feasibility (alias to concentrate highly charged adsorbate molecules at the surface of core@shell AuNPs@polymer nanocomposites), 5,10,15,20-tetra-(*N*-methyl-4-pyridyl)porphyrin (TMPyP) was chosen as a model adsorbate in the present work. This porphyrin per se [23], or in conjunction with carbon dots [24], AuNPs [25] and/or Au (III) ions [26] is known to serve as a sensitizer in photodynamic therapy (PDT) of cancers and/or as antitumor agent, respectively. It is a tetracationic porphyrin that is incapable of forming aggregates and/or dimers in its low concentrations in an aqueous solution [12,27,28] due to the electrostatic repulsion of four positive charges; indeed, TMPyP stays non-aggregated until 1 mM concentration value [27]. It can be easily measured by UV–vis, fluorescence, and RRS/SERRS spectroscopies (exploiting resonance with its electronic absorption when appropriate excitation laser line chosen). In tumour-related applications, TMPyP is usually employed in the concentrations of units and dozens of micromolar [23–26]. Therefore, it is utmost important to detect TMPyP in such concentrations (1 μM and lower) unequivocally, which is the right task for RRS/SERRS. The choice of TMPyP as a model adsorbate in this study is not random, but rather based on our previous experiences with it [28–32]. To the best of our knowledge, here, it is also the first time when TMPyP is detected based on its preconcentration in the close vicinity of Au@thermoresponsive polymer nanocomposites.

TMPyP is known to form J- and H-aggregates under very specific conditions [12,28,33]; the former type of aggregates causes higher fluorescence quenching than the latter [12]. Besides PDT of cancers, TMPyP has been exploited by many authors for other applications; it served so far as: (i) photoactive compound producing singlet oxygen in electrospun nanofibers exploited as antibacterial substrates [34], (ii) bactericidal agent against *Staphylococcus aureus* when sensitized by farnesol and activated upon red light [35], (iii) reversible proteasome inhibitor [36], (iv) telomerase inhibitor [37], and (v) optical sensor for the toxic heavy metal ions detection in aqueous solutions [38].

Based on the concentration range frequently used in cancer-related applications, low TMPyP concentrations (0.1 and 1 μM) were investigated here to prove the proposed new concept. If TMPyP concentrated (i.e., aggregated) at the surface of Au@polymer nanocomposites (although the final TMPyP concentration in aqueous solution does not exceed the calculated monolayer surface coverage concentration value), its aggregates can be easily recognized by (a) UV–vis absorption spectroscopy (by Soret band shifts), (b) fluorescence signal quenching and changes of fluorescent features, and (c) SERRS signal detection of TMPyP aggregates spectral form, as demonstrated within this study. Moreover, the thermoresponsiveness of the smart polymers augmented the J-aggregates formation of TMPyP at slightly elevated temperatures as assumed. Furthermore, the long-term stability of the SERRS signal of the porphyrin was achieved (as evidenced by 1-month aged samples) due to the presence of the smart polymer shell that surrounds the plasmonic Au core and prevents AuNPs aggregation. Apart from spectroscopic methods, many other experimental techniques, such as transmission electron microscopy (TEM), dynamic light scattering (DLS), zeta potential measurement, and inductively coupled plasma mass spectrometry (ICP-MS) were employed for the characterization and investigation of the nanocomposites under study, and their interaction with the cationic porphyrin selected as a model compound.

2. Materials and methods

2.1. Chemicals

Gold (III) chloride hydrate (Aldrich, 99.999 % trace metal basis), sodium citrate (Sigma-Aldrich, p.a., ≥ 99.0 %), sodium borohydride (Fluka, ≥ 99 %); 5,10,15,20-tetra-(*N*-methyl-4-pyridyl)porphyrin (TMPyP, Sigma-Aldrich, 97 % dye content). All stock solutions were prepared with deionized water (purification system Milli-Q, Millipore Corp., Bedford, MA, USA). All glassware was cleaned with aqua regia acid (the mixture of nitric acid and hydrochloric acid in the ratio of 1:3) and copious amounts of deionized water before its usage.

The monomers, 2-(2-methoxyethoxy)ethyl methacrylate (MEO_2MA, Aldrich 95 %) and *N*-isopropylacrylamide (NIPAM) were purified by passing through a neutral alumina column and recrystallization, from a hexane/toluene mixture (90/10 vol%), respectively; Styrene (St, Merck > 99 %) and methyl methacrylate (MMA, Merck > 99 %) were used as received. The chemicals, 2-(2-(2-(acetylthio)ethoxy)ethoxyl)ethyl methacrylate ($AcSEO_2MA$), 2-(2-(2-chloroethoxy)ethoxy)ethan-1-ol (96 %, Aldrich), methacryloyl chloride (97 %, Aldrich), triethylamine (99 %, Scharlau), dichlorometane (DCM) (99 %, Aldrich), anhydrous sodium sulfate (99 %, Qemical), potassium iodide (99.5 %, Panreac), potassium thioacetate (98 %, Aldrich) and acetonitrile (99.9 %, Scharlau) were employed as received. The reagents, [1,1,4,7,10,10-hexamethyltriethylene-tetramine (HMTETA) (97 %, Aldrich); copper chloride (CuCl) (≥99.99 %, Aldrich); ethyl-2-bromoisobutyrate (EBriB) (98 %, Aldrich); ammonium persulfate (APS) (>98 %, Fluka); tetraethylene glycol dimethacrylate (TEGDMA) (>90 %, Fluka); sodium dodecyl sulfate (SDS) (Fluka). Solvents were dried by standard methods or by elution through a Pure Solv Innovative Technology column drying system. Additional chemicals needed for the preparation of non-plasmonic referent systems: Ethanol absolute and toluene were purchased at Scharlau. Hydrochloric acid (37 %) was supplied by VWR. Tetraethyl orthosilicate (TEOS),3-(trimethoxysilyl)propyl methacrylate (TMSPMA, 98 %) were provided by Sigma Aldrich. Triethylamine was from Acros Organic, Ammonium hydroxide (NH_4OH, 25 %) was supplied by Panreac.

2.2. Synthetic procedures

2.2.1. Synthesis of Au@polymer core@shell nanocomposites

The Au@p(MEO_2MA) nanocomposites were synthesized following the synthesis described below for sample Au20PM. In a Pyrex tube equipped with a magnetic stirrer and an N_2 gas inlet, 2 mL of as-prepared P(MEO_2MA-co-AcSEMA) capped Au NPs aqueous solution was heated to 70 °C, followed by the addition of MEO_2MA monomer (0.138 mmol), TEGDMA cross-linker (4.12 × 10¯3 mmol), and SDS (1.145 × 10¯3 mmol) under stirring to form a homogeneous solution. After a 20 min N_2 purge, polymerization was initiated by adding 100 μL of APS solution (0.035 M).

The Au60PN and Au60PS nanocomposites were synthesized through the procedure defined below for sample Au60PN. In a tube equipped with a stirrer and an N_2 gas inlet, reactive were added as follows: $AcSEO_2MA$ monomer in ethanol (1.72 10^{-3} mol), NIPAM monomer (6.4 10^{-2} mmol), TEGDMA crosslinker (1.71 10^{-3} mmol), ethanol, SDS in water (2.9 10^{-4} mmol) and 1 mL of citrate capped Au NPs aqueous solution under stirring. After 20 min N_2 purge, polymerization was initiated by heating up to 70 °C, followed by the addition of 100 μL of APS solution (0.02 M).

In both procedures, the reaction was stopped after 2 h, by cooling down in an ice bath while the tube was opened to the air. Finally, after water dilution, the sample was 4× centrifuged (4600 rpm, 30 min) and re-suspended in water until the complete removal of empty polymer micelles and excess reactants.

2.2.2. Preparation of Au@polymer nanocomposite-TMPyP systems

Two final concentrations of TMPyP were used: 1 μM (labelled as TMPyP6) and 0.1 μM (labelled as TMPyP7). Both were investigated by SERRS measurements, while only 0.1 μM in fluorescence measurements. The Au@polymer nanocomposite-TMPyP6 and/or -TMPyP7 systems for SERRS measurements were prepared by addition of 8.5 μL of 1×10^{-5} M and/or 1×10^{-6} M TMPyP solution to 75 μL of the appropriate Au@polymer nanocomposite, respectively. Reference systems containing TMPyP6 and TMPyP7 were prepared in a similar way, just 75 μL of deionized water was used instead of the appropriate nanocomposite solution.

2.3. Methods of characterization

2.3.1. UV–Vis spectra

UV–Vis spectra of the nanocomposites, as well as systems with TMPyP6 were recorded on spectrometer Specord PLUS 250 (ChromSpec, Analytic Jena, Jena, Germany), in the range between 190 and 1100 nm. Quartz cuvettes with 1.35 mL of a particular colloidal sample were used for the measurements. Deionized water in another quartz cuvette served as a reference.

2.3.2. DLS and Zeta potential measurements

Hydrodynamic diameters and zeta potentials were measured with a Zetasizer Nano ZS instrument (Malvern Instruments Ltd., UK) equipped with a 4 mW He-Ne laser operating at a light source wavelength of 632 nm and a fixed scattering angle of 173° for detection. Malvern Dispersion Software was used for data acquisition and analysis, applying the general-purpose algorithm for calculating the size distribution.

2.3.3. Fluorescence spectra

Fluorescence spectra were recorded on a JASCO F8500 (Jasco, Tokyo, Japan) spectrofluorometer using a 1 cm quartz cuvette and 2.5 nm slits. The excitation wavelength was set to 422 nm. Emission spectra were

measured in the range of 600–850 nm with the scan speed of 100 nm/min, high sensitivity, and 0.1 nm data interval. Three scans were averaged to provide a representative spectrum which was further smoothened (adjacent average). All spectra were corrected to avoid any deviations induced by instrumental components. Deionized water served as a blank. Due to the necessity of higher volume than 83.5 μL, samples were prepared as follows: 70 μL of SERRS-samples (containing 1×10^{-6} M TMPyP, abbreviated as TMPyP6) were added to 630 μL of deionized water, resulting thus in 1×10^{-7} M final TMPyP concentration (TMPyP7).

2.3.4. Resonance Raman and surface-enhanced resonance Raman spectra

Resonance Raman and surface-enhanced resonance Raman spectra were acquired on a Raman Optical Activity spectrometer developed at Palacký University Olomouc. Liquid samples were measured in a rectangular fused quartz cell of 70 μL volume placed in a temperature-controlled box, using the back-scattering geometry, scattered circular polarization (SCP) modulation scheme, and Nd:YAG laser with 532 nm excitation wavelength. Laser power of 10 mW, accumulation time of 2.5 s, 16 scans, and 12 frames were employed. The RRS/SERRS spectra were recorded at room temperature (20 °C), or 15 °C, and/or 32 °C. *prior* to RRS/SERRS spectra acquisition at the defined temperatures, the delay time was 8 min to enable the particular sample to be temperature-equilibrated. The RRS/SERRS spectra recorded at 532 nm excitation laser line were measured in two-three independent measurements at 15, 20, and 32 °C, separated by a period of 8 months in several cases. Since the repetition provided the same signal patterns and the same trends, it could be concluded that the nanocomposites are stable in the course of time. It should be noted that SERRS was measured at 15 °C rather than at 12 °C (the case of DLS measurements) to avoid high humidity problems (resulting in bedewing of cuvettes). The choice of excitation laser line is further discussed in Supporting Information.

2.3.5. Inductively coupled plasma mass spectrometry (ICP-MS)

To accurately determine the total Au content, the validated ICP-MS method was employed. Prior to ICP-MS analysis, each sample was sonicated and consequently digested using an MLS 1200 M closed vessel microwave digestion unit (Milestone, Italy). The organic matrix was decomposed by a mixture of 4 mL of nitric acid (69 %, Analpure) and hydrochloric acid (36 %, Analpure) in 1:1 ratio. The digests were allowed to cool down to laboratory temperature, diluted with the ultrapure water to 25 mL in volumetric flasks, and stored at 4C until ICP-MS analysis. The detailed ICP-MS method description and the corresponding validation in terms of the limit of detection (LOD), the limit of quantification (LOQ), trueness, and precision are presented in the Supplementary Materials of our previous work [39]. All ICP-MS measurements were performed in triplicates, and the results are expressed as an average ± standard deviation (SD).

2.3.6. Transmission electron microscopic (TEM)

Transmission electron microscopic (TEM) imaging were performed by using a Jeol 2010F transmission electron microscope (Jeol USA, Inc., Peabody, MA, USA), equipped with a LaB6 cathode (accelerating voltage 30 kV–200 kV; CCD camera KEENview G2 (ResAlta Research Technologies, Golden, CO, USA). A 3-μL drop of a particular colloidal sample was deposited onto a carbon-coated copper grid. Grids were allowed to dry at room temperature in a Petri dish covered by its lid for at least one day before performing TEM measurements. Energy dispersive spectra (EDS) of selected samples were recorded on Oxford x-MAX 80 T (SSD) (Oxford Instruments, Oxford, UK).

3. Results and discussion

The interaction of a cationic porphyrin (TMPyP) in therapeutically-important concentrations (1 μM) with nanocomposites, differing in the polymeric shell surrounding plasmonic Au nanoparticle core (AuNPs, 60 nm in diameter, abbreviated as Au60), was investigated by using spectroscopic techniques. The nanocomposites are labelled as follows: Au60PS (polystyrene at AuNPs of 60 nm in diameter), Au60PN (poly-N-isopropyl-acrylamide at AuNPs of 60 nm in diameter), Au60PM (poly-2-(2-methoxy-ethoxy)ethyl- methacrylate at AuNPs of 60 nm in diameter). Chemical structures of the three different polymeric shells formed and cross-linked around AuNPs core are given in Scheme 1.

In the case of $pMEO_2MA$, the impact of the plasmonic core of sizes 20 and/or 100 nm in diameter embedded in the smart polymeric shell, named Au20PM and Au100PM, respectively, on properties and potential applicability for TMPyP detection were looked into as well.

The microscopic morphologies of all five Au@polymer nanocomposites before their interaction with TMPyP are shown in Fig. 1. It reveals the concentric and/or eccentric polymeric shells around AuNPs in the cases of thermoresponsive polymers; while Janus type of particles in Au60PS nanocomposite. Concerning particle size distribution (PSD) derived from TEM images, the reader is referred to the Supporting Information (Table SI-1 and Figure SI-1). However, it should be kept in mind that TEM images are recorded in dried state; whereas spectroscopic measurements are performed in solution. Therefore, dynamic light scattering (DLS) is also measured and the results, expressed as hydrodynamic diameters, considered when monolayer surface-coverage concentration (MLSCC) of the model adsorbate calculated for instance.

In the following text, we focus our attention first on the effect of each polymeric shell around the AuNP core (of 60 nm in diameter) on nanocomposite characteristics while interacting with TMPyP. In the second part, the influence of plasmonic AuNP core size (20 nm and/or 100 nm) on the detection of TMPyP, while using the same polymeric shell ($pMEO_2MA$), is addressed.

3.1. TMPyP interaction with AuNPs (60 nm in diameter) surrounded by three different polymeric shells

TMPyP is a chromophore molecule possessing characteristic absorption bands in the visible part of electromagnetic radiation, i.e., intensive Soret band around 423 nm and four Q-bands located at 518, 556, 586, and 642 nm [28]. Plasmonic AuNPs manifest themselves by surface plasmon extinction (SPE) band occurring also in the visible region. Therefore, we recorded UV–vis spectra of nanocomposites before and after their interaction with TMPyP molecules in the range of 350–800 nm, Figures SI-2 A-2E. For the sake of a direct comparison, the interaction of TMPyP with AuNPs without any polymeric shell, prepared by commonly used methods (citrate- and borohydride-induced reductions), was followed by UV–Vis spectroscopy and the spectra are shown in Figures SI-2F-2H as well. Since the final TMPyP concentration in all systems with nanocomposites is of 1 μM value (as labelled by number 6 behind the TMPyP abbreviation), only the Soret band can be clearly distinguished in the UV–vis spectra; while Q bands stemming from TMPyP are overlapped by particular SPE band of a nanocomposite. The position of SPE and Soret band maxima for each system (meaning the nanocomposite and nanocomposite-TMPyP6) are summarized in Table 1.

Based on UV–Vis spectra (Figures SI-2), it is obvious that AuNPs without polymeric shells tend to aggregate while interacting with TMPyP6 (which results in red-shift and broadening of SPE band), whereas AuNPs with polymers around plasmonic Au core do not. The position of the characteristic SPE band is only one feature among others (like band intensity, band shape, etc.), which describes the interaction between plasmonic nanoparticles and an adsorbate molecule. However, for clarity of presentation and excluding aggregation of polymer@Au nanocomposites, we can focus on it solely. Thus, as demonstrated in Table 1, the addition of TMPyP to Au60 nanocomposites with three distinctly different polymeric shells resulted in virtually no changes in SPE band positions. This was confirmed by visual control as well; no AuNPs aggregation was observed by the naked eye, and the character of proper solutions was preserved.

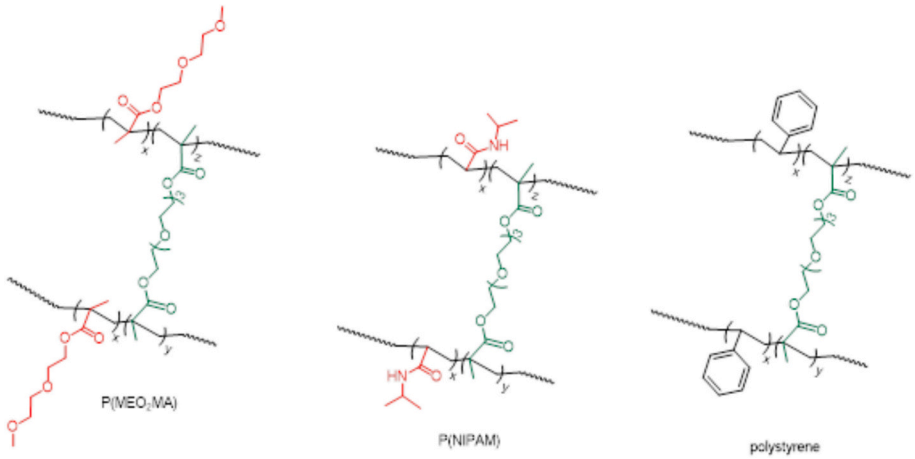

Scheme 1. Chemical structures of polymeric species surrounding AuNPs used in this study.

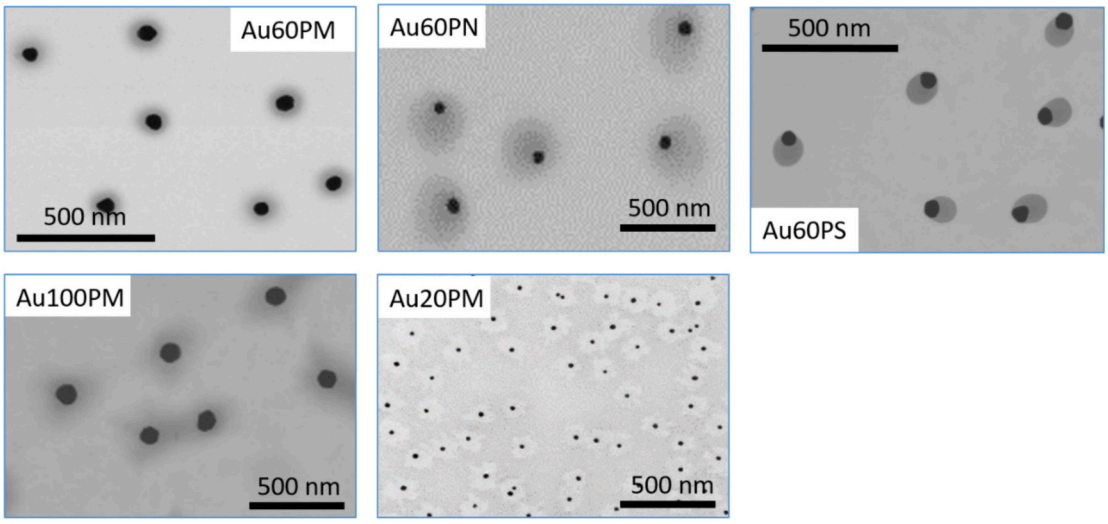

Fig. 1. Morphologies of the Au@polymer nanocomposites before their interaction with TMPyP. Concentric shells are grown in the cases of Au60PM, Au100PM, and Au20PM; while eccentric growth of the polymeric shell is used in Au60PN and Au60PS.

Table 1
Changes in the position of maxima of SPE band stemming from AuNPs in Au nanocomposites and Soret band of TMPyP.

nanocomposite	λ_{max}(SPE) [nm]	Addition of TMPyP[£]	
		λ_{max}(SPE) [nm]	λ_{max}(Soret) [nm]
Au60PS	565	565	424
Au60PN	559	560	426
Au60PM	564	564	431
Au20PM	527	529	429
Au100PM	581	585	433

Note: [£]Soret band of TMPyP is positioned at 423 nm. The experimental error is ±1 nm.

On the contrary, the Soret band of TMPyP (positioned at 423 nm for the monomeric porphyrin) is slightly or substantially red-shifted in Au60PN-TMPyP6 or Au60PM-TMPyP6 systems, respectively – Table 1; definitely beyond the experimental error which is ±1 nm. As known from the literature [33], TMPyP aggregates containing multiple porphyrin molecules can be formed upon their interaction with a surfactant (dissolved in aqueous solution in its premicellar concentration value) that is negatively charged (e.g., SDS). The Soret and Q bands are then red-shifted by a few nanometers [33]. We deduce that the red-shift of TMPyP Soret band observed in our Au@polymer nanocomposites may report about J-aggregates formation of porphyrin molecules interacting with the polymeric shell of the Au60 nanocomposites. In our previous work [28], J-aggregates formation of TMPyP was also encountered in the presence of borohydride anions and/or hydroxide (basic medium), which both represent quite dissimilar environments than here, where a polymeric shell (namely $pMEO_2MA$) most probably leads to J-aggregates of TMPyP formation.

Zeta potential values of each Au60 nanocomposite before and after the interaction with TMPyP molecules are listed in Table SI-2. All Au60 nanocomposites manifested themselves by negative zeta potentials ranging between −14 and − 23 ± 7 mV; the most negative being encountered in Au60PM, while the least negative in Au60PS. There are very few changes, basically within the experimental error, in the average values for all three Au60 nanocomposites when allowed to interact with TMPyP (1 μM final concentration). Repulsive forces then keep the nanocomposites away from each other although cationic porphyrin molecules interact at their surface. It thus supports the spectroscopic results observed by UV–vis measurements, i.e., no obvious AuNPs aggregation and preservation of solution transparency.

As a sort of referent systems, namely for RRS spectroscopic measurements, nanocomposites consisting of silica core (60 and/or 100 nm) coated with thermoresponsive polymeric shells (PNIPAM and

PMEO$_2$MA) were synthesized and are labelled as SST60PN, SST100PN, SST100PM (details of their syntheses are described in Supporting Information, Section 4). UV–vis spectra of these non-plasmonic nanocomposites prior and after their interaction with TMPyP are shown in Figure SI-3. Apparently, there are no signs of Soret band shifts (see Figure SI-3). Further characteristics of the SiO$_2$@polymer core@shell nanocomposites, such as their representative TEM images and Fourrier transform infrared (FT-IR) spectra are shown in Figure SI-4; their zeta potential values prior and after the TMPyP addition are listed in Table SI-2 in Supporting Information.

The polymeric shell is thick enough as determined by TEM (Fig. 1, Table 2) and/or by DLS measurements (Table 2 and Tables SI-3, SI-4) to hinder the direct interaction between TMPyP and the metallic surface in Au@thermoresponsive polymer nanocomposites. It coincides well with the UV–Vis measurements: the polymeric shell well protects AuNPs, preserving their SPE maximum position. Furthermore, the size changes of Au@thermoresponsive polymer nanocomposites in solution (determined by DLS) as a function of temperature (Figure SI-5) are followed with the aim to determine the volume phase transition temperature (VPTT) of each particular system. The values derived from the size-temperature dependence (Figure SI-5) are then listed in Table SI-5 together with polymer shell swelling ratios. DLS results for the referent SiO$_2$@thermoresponsive polymer core-shell nanocomposites recorded at two temperatures (12 °C and 32 °C) are shown in Table SI-6.

Fluorescence spectra of TMPyP (in 0.1 μM final concentration, labelled TMPyP7) measured in deionized water and/or after the interaction with Au60 nanocomposites (excitation 422 nm in all cases) are shown in Fig. 2.

The characteristic fluorescence of porphyrin (labelled as TMPyP7) is quenched in all three Au60 nanocomposite-TMPyP7 systems. Fluorescence quenching is characteristic for aggregated porphyrins [12]. The order of nanocomposites according to increasing efficiency of TMPyP fluorescence quenching (derived from Fig. 2) is as follows: Au60PS < Au60PN < Au60PM. Moreover, the character of TMPyP fluorescence is changing from a central peak located at around 720 nm with a broad shoulder positioned at approx. 655 nm, into two well distinguished peaks of similar intensities, appearing at 660 and 720 nm. The observation of two well-separated peaks has been discussed in [12,27] already. It is explained by the decrease in the mixing of the porphyrin singlet excited state and charge transfer state (i.e., intramolecular charge transfer between Π-system of porphyrin macrocycle and pyridinium groups) in assembled TMPyP molecules [12,27]. Importantly, pristine Au60 nanocomposites (i.e., without TMPyP) manifested themselves by no fluorescence features in the emission region of interest, 600–850 nm - Figure SI-6.

Resonance Raman scattering (RRS) spectra of TMPyP and surface-enhanced resonance Raman scattering (SERRS) spectra of Au60 nanocomposite-TMPyP6 systems are shown in Fig. 3 and were recorded by using a 532 nm excitation laser line. Note that the RRS/SERRS spectra as measured are shown in Figure SI-7 A-B.

Table 2
Average polymeric shell thicknesses surrounding plasmonic Au cores as derived from DLS and/or TEM data (diameters are considered, i.e. regardless eccentric and/or concentric character of the shell).

Nanocomposites	Polymer shell thickness	Polymer shell thickness from DLS data (nm)	
	from TEM data (nm)	12 °C	32 °C
Au20PM	66	125	76
Au60PM	54	208	129
Au100PM	168	101	63
Au60PN	229	380	133
Au60PS	102	87	

Note: The given polymer shell thicknesses are obtained by subtracting the gold core diameter (determined by DLS, Z average value as listed in Table SI-4) measured by DLS. Thus, only the polymeric shell diameter (2R in concentric shell cases) without any gold core is summarized here. Similarly for the thicknesses derived from TEM data (summarized in Table SI-1).

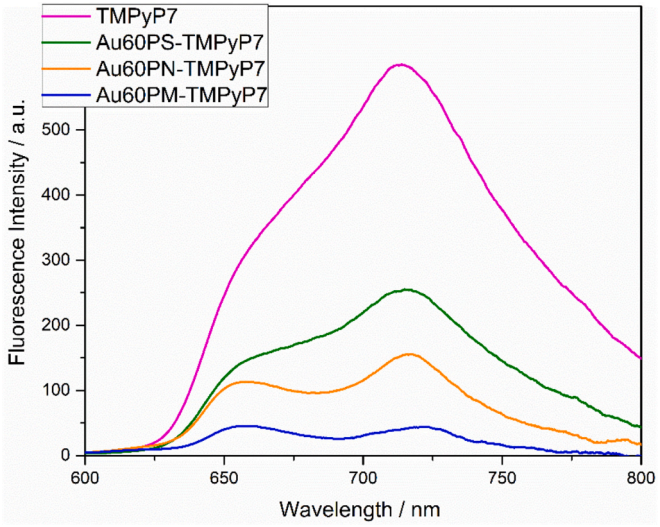

Fig. 2. Fluorescence spectra of TMPyP (0.1 μM final concentration, labelled as TMPyP7) in deionized water and/or in Au60@polymer nanocomposites. Excitation 422 nm.

It should be mentioned here that SERRS spectra are recorded at two different temperatures (15 °C and 32 °C) – compare Fig. 3A and B. These two temperatures, derived from the thermal responsiveness of the Au@polymer nanocomposites under the study as demonstrated in Figure SI-5, are chosen and correspond to distinctly different thicknesses of pNIPAM and pMEO$_2$MA around AuNPs, in accordance with our previous work [17]. When the temperature is below/above the polymers VPTT value (Table SI-5), they manifest themselves by changes in volume. Consequently, the hydrodynamic diameter of nanocomposites changes as demonstrated in Table 2 and Table SI-3: swelling of polymeric shell is encountered at temperatures below VPTT (measurements at 12 °C), while shrinkage of polymeric shell above VPTT (measurements at 32 °C).

When comparing peak positions in Fig. 3 with the literature [40], where peak assignment of TMPyP in RRS and SERRS spectra can be found, the characteristic RRS spectrum of TMPyP is validated (Fig. 3A). On the other hand, SERRS spectral features of TMPyP interacting with Au60 nanocomposites resemble qualitatively to so-called SERRS spectral form III of TMPyP [41] regardless the type of polymer shell surrounding Au core. Namely, the peaks located at 385 cm^{-1}, 1368 cm^{-1}, and a shoulder at 1015 cm^{-1} (Fig. 3A), are the three most prominent characteristics of SERRS spectral form III of TMPyP. The appearance of this TMPyP spectral form is very surprising in systems containing Au core and polymeric shell because it has been detected solely as a surface complex of TMPyP adsorbed on AgNPs so far, i.e., assigned to the surface complex of Ag-TMPyP [41]. Here, except Au core in nanocomposites (which, if uncovered by polymers, can interact with TMPyP revealing the characteristic SERRS signal as shown in Figure SI-7C), no Ag and/or any other metal is present as validated by ICP-MS measurements. Moreover, the thermoresponsive polymeric shell surrounding the Au60 core is quite thick (Table 2), hence, any direct interaction between the porphyrin molecules and gold can be excluded as well (namely in Au60PM and Au60PM). Based on UV–Vis spectra and fluorescence features, we assume that J-aggregates are rather responsible for the observation of this type of SERRS spectral form in the Au60@polymer nanocomposite-TMPyP6 systems. Indeed, the tentative assignment of SERRS spectral form III of TMPyP to Ag-TMPyP in the previous work [41] should be reconsidered. In fact, the same stretching and bending deformations of TMPyP could be attributed not only to metallation, but also to stacking of porphyrin molecules as stated in [42]. Diacidic form

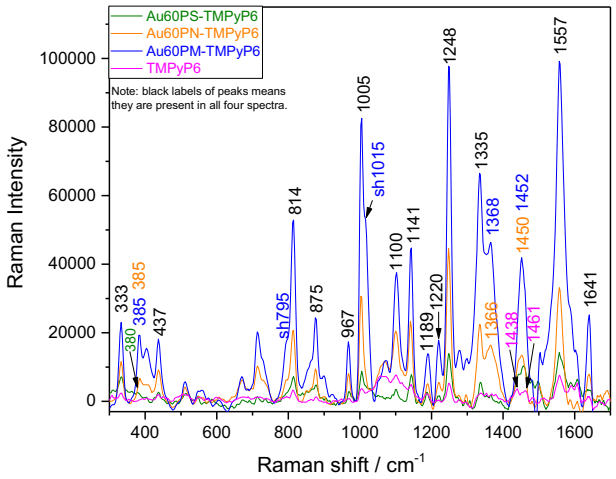

A

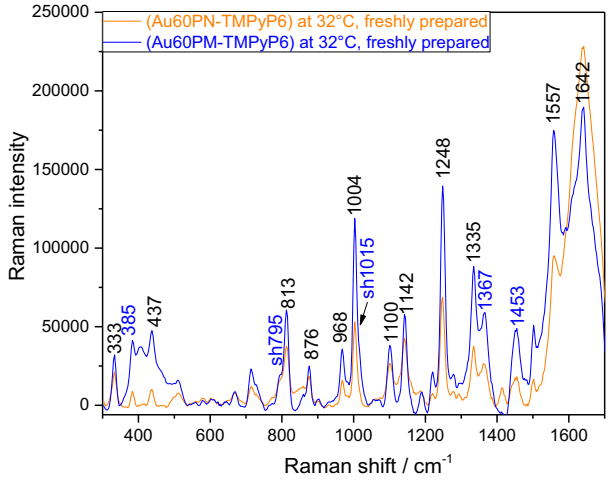

B

Fig. 3. (A) RRS spectrum of TMPyP6 (after water subtraction and baseline correction) and SERRS spectra of the AuNP@polymer-TMPyP6 systems (after appropriate background subtraction and baseline correction) as specified in insets (measurements at 15 °C). (B) SERRS spectra of selected systems recorded at 32 °C. Excitation laser line 532 nm in all cases.

of TMPyP can be excluded from considerations because its RRS spectral pattern looks differently (Figure SI-7D).

Generally, aggregate formation of molecules at NP surfaces can be envisaged in systems where the molecular concentration exceeds the monolayer surface-coverage concentration (MLSCC) calculated for a particular NP surface. Hence, we tried to estimate the MLSCC of TMPyP on each Au60@polymer nanocomposite, while considering the real hydrodynamic diameter of Au60@polymer nanocomposites and the real counts of AuNPs within each system (see Supporting Information sections 10 and 11 for details). ICP-MS data determined the average content of Au (in μg/L) in each nanocomposite (Table SI-7). Consequently, theoretical calculations could be performed to estimate the MLSCC of TMPyP on Au60@polymer nanocomposites (Table SI-8). The measured final TMPyP concentration (1 μM) obviously does not exceed the MLSCC value of TMPyP on Au60PM and Au60PN at temperatures below VPTT (SERRS measured at 15 °C), whereas MLSCC of TMPyP is around this value on Au60PN at temperatures above VPTT (SERRS measured at 32 °C) and exceeded on Au60PS. Therefore, it is surprising that J-aggregates of TMPyP can be formed in all three nanocomposites. Nevertheless, the direct interaction between TMPyP and polymeric chains considered on the molecular level, similarly as in [12], may be responsible for the unique phenomenon of J-aggregates formation of TMPyP even though the MLSCC is not reached and overcome.

As a further proof of TMPyP aggregates formation induced by the presence of polymeric shell around the plasmonic core, RRS spectra of TMPyP (1 μM final concentration) on nonplasmonic SiO_2@thermoresponsive polymer nanocomposites (labelled as SST60PN-TMPyP6, SST100PN-TMPyP6, SST100PM-TMPyP6) were recorded under the same conditions as SERRS spectra of TMPyP on plasmonic Au60@polymer nanocomposites (Figure SI-8). Obviously, the RRS/SERRS spectral form, characterized by 384 cm^{-1} etc., is repeatedly encountered. It thus confirms the generation of TMPyP J-aggregates at polymeric shells composed of pNIPAM and $pMEO_2MA$ surrounding any core, nonplasmonic as well as plasmonic. Based on the particular characteristics (namely TEM images and zeta potential values) of the plasmonic Au60@polymer nanocomposites and considering the chemical composition of polymeric shells (structures shown in Scheme 1), a mechanism of TMPyP aggregation can be envisaged as depicted in Scheme 2.

We assume that the main driving force for the cationic porphyrin interaction with plasmonic Au60@polymer nanocomposite surfaces (negatively charged) is a coulombic attraction. Furthermore, each cationic porphyrin has its hydration envelope moving together with the tetra-cation to the close vicinity of the negatively charged surface of core@shell nanocomposites. There, the amphiphilic character of the polymeric shells in the case of pNIPAM and $pMEO_2MA$ (as proven in [43,44], respectively), while negatively charged parts of the surface in Au60PS comes into the play and causes sticking of the tetra-cation with its hydration envelope onto the nanocomposite surface to a higher and/or smaller degree according to the hydrophilicity of the particular polymer. It is known that pNIPAM segments are more hydrophobic than $pMEO_2MA$ segments [45]. It is also reasonable to assume that pSTYRENE is the most hydrophobic polymer from the three used in the present study, when taking into account the results of contact angle measurements done in ref. [46] for pSTYRENE and other polymers including poly(methyl methacrylate). Due to the negative charges at nanocomposite surface (stemming from the citrate and its residues), the tetra-cation can be compensated enabling thus the interaction of another tetra-cation that is stuck into the polymeric shell in the same way as the former one. By this way, porphyrin molecules can aggregate step-by-step and create J-aggregates at the surface of core@polymeric shell nanocomposites regardless the character of the core (either plasmonic, or non-plasmonic).

Furthermore, there is a question about the J-aggregates size (under the assumption that each aggregate is composed of countable TMPyP molecules) since it may vary from system to system as it can be deduced from UV–vis spectra already (i.e., different shifts of Soret band maximum: negligible in Au60PS-TMPyP and, on the contrary, the most pronounced in Au60PM-TMPyP). There may be trimers of TMPyP in Au60PS according to the approx. Trice abundance of TMPyP (i.e., the TMPyP concentration exceeding three times the calculated MLSCC value, Table SI-8). As for Au60PN-TMPyP6 and Au60PM-TMPyP6, the MLSCC value is not exceeded, but according to SERRS spectra, J-aggregates are formed even at low temperatures (15 °C), meaning that TMPyP is (pre)concentrated due to its interaction with pNIPAM and $pMEO_2MA$ polymeric shells most probably by the above suggested mechanism (Scheme 2). The process of J-aggregates formation is more pronounced in the latter case which is not surprising because of a systematically more negative zeta potential values encountered for $pMEO_2MA$ polymeric shells on plasmonic as well as non-plasmonic core@shell nanocomposites (Table SI-2).

To validate the J-aggregates formation in TMPyP concentrations well below MLSCC, one order of magnitude lower TMPyP concentration (0.1 μM) was also measured on the selected nanocomposite (Au60PM) - Figure SI-9. The same SERRS spectral features were detected (compare the spectrum in Figure SI-9 with that shown in Fig. 3A). This means, in turn, that J-aggregates are generated even though the final TMPyP

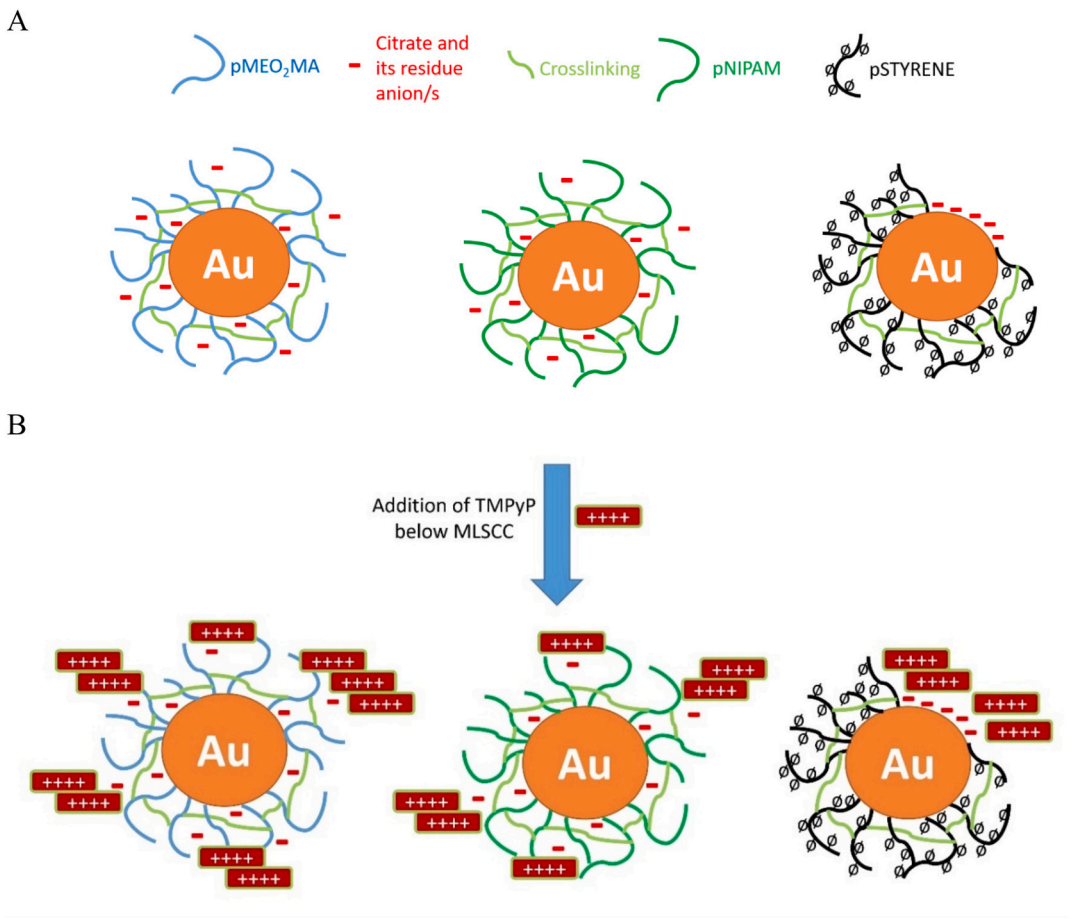

Scheme 2. (A) Depiction of different types of Au@polymer nanocomposites taking into account their composition, zeta potential values, and polymeric shell arrangements as derived from experimental measurements. Negative charges stem from citrate and its residues. Cross-linking polymer is also schematically depicted. (B) Spontaneous J-aggregates formation of the tetra-cationic porphyrin at the surface of these Au@polymer nanocomposites.

concentration is much lower than the estimated MLSCC value for TMPyP and Au60PM (4 μM at 12 °C and/or around 2 μM at 32 °C). Therefore, the direct intermolecular interaction of polymeric shell with TMPyP molecules is of the utmost importance and leads toward J-aggregation of cationic porphyrin molecules in the close vicinity of the nanocomposite surface. This may be envisaged as a completely new approach toward cationic porphyrins (representing a model adsorbate) detection at their low concentrations (therapeutically used values and even below to detect any residual molecules) due to their preconcentration which is achieved owing to the TMPyP interaction with polymeric shell (namely $pMEO_2MA$). In general, it could potentially work for any other organic species (e.g., pollutants/drugs/biomolecules) if appropriate molecular interaction occurs between the organic species of interest and the polymeric shell of the nanocomposites.

By careful studying the available literature, H-aggregates of TMPyP have been detected on a polyanionic matrix of inorganic polyphosphate [12]. However, 10 or even 50 μM TMPyP final concentrations were employed in their case. Historically, there have been even concerns about the spontaneous aggregation of TMPyP molecules in aqueous solutions at low concentrations (0.1 μM) and discrepancy in threshold values of TMPyP aggregation concentration [27]. In ref. [27], the authors gave evidence that controversial results obtained by different authors could be explained by taking (i) the adsorption of TMPyP onto solid surfaces (e.g., walls of the quartz cuvette) or solid impurities (related to the quality of distilled water) and (ii) differences in experimental arrangements into account. It can be assumed that the polymeric surface of our nanocomposites represents the suitable solid surface, which supports TMPyP aggregation. Then, the extent of TMPyP aggregation is directed by the type of polymeric shell on the plasmonic Au core (as evidenced in Fig. 3). The order of polymeric shells used in this study and supporting TMPyP aggregation (preconcentration) can be arranged as it follows: $pMEO_2MA$ > pNIPAM > pSTYRENE. This order could be related to the degree of polymers hydrophobicity [45,46], increasing when going from $pMEO_2MA$ through pNIPAM to pSTYRENE.

Quantitatively, Raman signal intensity increases at least by one order of magnitude in Au60PN-TMPyP6 and Au60PM-TMPyP6 systems in comparison to RRS signal of TMPyP in deionized water (1 μM final TMPyP concentration in all systems measured at 15 °C) – Fig. 3A. It should be noted that the overall signal intensity of TMPyP at SiO_2@-polymer nanocomposites (Figure SI-8 A-C) is roughly the same as that of TMPyP6 in pure water, meaning that no enhancement of RRS by non-plasmonic nanocomposite surfaces is observed. Therefore, despite the thickness of the polymeric shell around the plasmonic core in Au60PN and Au60PM being quite large (Table 2), there is still an enhancement coming most probably from SPE. When SERRS was measured at 32 °C (Fig. 3B), under otherwise identical experimental conditions, a further increase by roughly 1.7× and 1.5× (considering characteristic peak at 1005 cm^{-1}) in Raman scattering signal of TMPyP on Au60PN and Au60PM is achieved, respectively. This can be explained by the thermo-sensitivity of pNIPAM and $pMEO_2MA$ polymeric shells; both polymers can decrease their thickness around the Au core by the temperature increase – Table 2, Table SI-3 and Figure SI-5. On the contrary, no RRS enhancement of TMPyP signal is observed in SiO_2@polymer nanocomposites while measuring at 32 °C (Figure SI-8D-F). This further corroborates the idea that plasmonic enhancement is observed in Au@thermoresponsive polymer core@shell nanocomposites, whereas

such an enhancement on SiO_2@polymer nanocomposites is missing.

Moreover, because of a polymeric shell shrinkage at elevated temperatures (here at 32 °C), SPE maxima of Au60 nanocomposites are blue-shifted (as shown in [17]) which leads to a better resonance of Au60polymer-TMPyP6 systems with the excitation laser line employed for SERRS measurements (532 nm). Simultaneously, while polymeric shell thickness decreases, porphyrin molecules (adsorbate in general) can better "feel" the surface plasmon stemming from the metallic core of plasmonic NPs. Moreover, by increasing the temperature, mobility (e.g. Braunian motion) of TMPyP molecules increases as well, resulting thus in a higher degree of potential collisions of porphyrin molecules and their aggregation. Hence, while the polymer shell shrinkage, pre-concentration of TMPyP is even more pronounced. It can be considered as the second step of TMPyP aggregation induced by thermoresponsive shell around the plasmonic core – as schematically depicted in Scheme 3.

All the above-mentioned reasons most probably support the increased signal intensity observed in SERRS spectra of TMPyP recorded at 32 °C on Au60PN and Au60PM nanocomposites in comparison to those recorded at 15 °C (compare the appropriate spectra in Fig. 3A and B). In other words, and to sum up, the Au60@polymer nanocomposites are active plasmonic substrates for SERRS detection of TMPyP J-aggregates at near physiological temperatures which is important when a therapeutically-active compound measured.

Generally, the long-term stability of Au nanocomposites can be assumed, especially when plasmonic Au core is embedded in a thick polymeric shell, which serves as a protecting envelope. However, once nanocomposites interact with an adsorbate, the situation can dramatically change; there can be dynamic processes of adaptation to different (new) environments. Therefore, it is important to investigate the ageing of Au60@polymer nanocomposite-TMPyP systems. Since SERRS spectroscopy is more sensitive than the other spectroscopic techniques (e.g., UV–vis), we measured SERRS spectra of Au60@polymer nanocomposite-TMPyP systems after a month of ageing (samples stored under dark at room temperature) – Fig. 4; spectra were recorded under otherwise the same experimental conditions as those shown in Fig. 3 and can be thus mutually compared.

The characteristic peaks of SERRS spectral form III (J-aggregates of TMPyP) are more intensive after one-month ageing of Au60@polymer nanocomposite-TMPyP6 systems (particularly in the case of $pMEO_2MA$ and pNIPAM). SERRS data thus show that J-aggregates of TMPyP are further developed at the surface of Au60@polymer nanocomposites in the course of system ageing. To quantify it easily, we determined mutual intensity ratios of selected peaks (333, 385, and 1005 cm^{-1}) for freshly prepared and 1-month-aged systems, i.e., intensities of markers of J-aggregates vs. free base form of TMPyP - Fig. 5: I(385 cm^{-1})/I(333 cm^{-1}) and I(385 cm^{-1})/I(1005 cm^{-1}). The former is the ratio of deformation vibrations of the porphyrin macrocycle and *N*-methylpyridinium group (located at 385 cm^{-1} [40]) vs. deformation vibrations of porphyrin macrocycle (at 333 cm^{-1} [40]). It thus reflects mostly

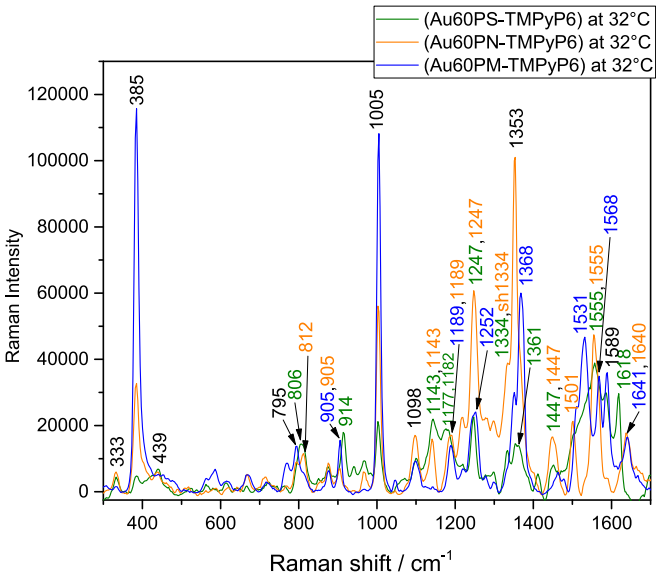

Fig. 4. SERRS spectra of the AuNP@polymer-TMPyP6 systems (after appropriate background subtraction and baseline correction) as specified in insets, after 1-month ageing, recorded at 32 °C, using a 532 nm excitation laser line.

changes in the deformation of the *N*-methylpyridinium group. The latter represents the ratio of deformation vs. symmetric stretching vibrations (at 1005 cm^{-1} [40]) of porphyrin.

It is evident that in the freshly prepared systems (Fig. 5A), both intensity ratios follow the same trend when going from Au60PS-TMPyP6 through Au60PN-TMPyP6 to Au60pPM-TMPyP6. On the contrary, in one-month-aged systems (Fig. 5B), the trends of intensity ratios split: it starts to be significant for the Au60PN-TMPyP6 case and is most pronounced for Au60PM-TMPyP6 (note: the scale of the y-axis is logarithmic in Fig. 5). Based on these results, it can be deduced that J-aggregates formation of TMPyP is enabled and continues to the greatest extent in Au60PM-TMPyP6, followed by Au60PN-TMPyP6 system during their ageing. Thus, the kinetics of J-aggregates formation of TMPyP differs on the three polymeric shells under investigation. Moreover, the extent of the deformation of *N*-methylpyridinium group (which is the career of positive charge in the studied porphyrin) observed in systems aged for 1 month can be arranged into the following order (starting from the most prominent one): Au60PM > Au20PM > Au100PM > Au60PN (Fig. 5B – note: logarithmic scale of intensity). It gives evidence about the dynamic rearrangement of this particular TMPyP part adapting to the hydrophilic segments within the polymer shell. This further supports the idea about the origin of TMPyP aggregation induced by direct molecular interaction with the polymeric shell of nanocomposites because all nanocomposites containing $pMEO_2MA$ shell are before the one consisting of pNIPAM in the above derived order.

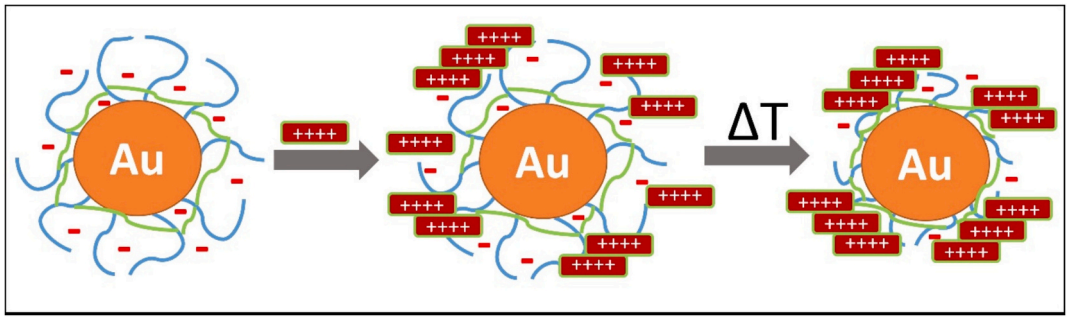

Scheme 3. Depiction of the two-step TMPyP aggregation (i.e., J-aggregates formation). The first step is the spontaneous TMPyP aggregation induced by the polymeric shell (the mechanism suggested in Scheme 2); whereas the second step is caused by the thermal responsiveness of the polymeric shell.

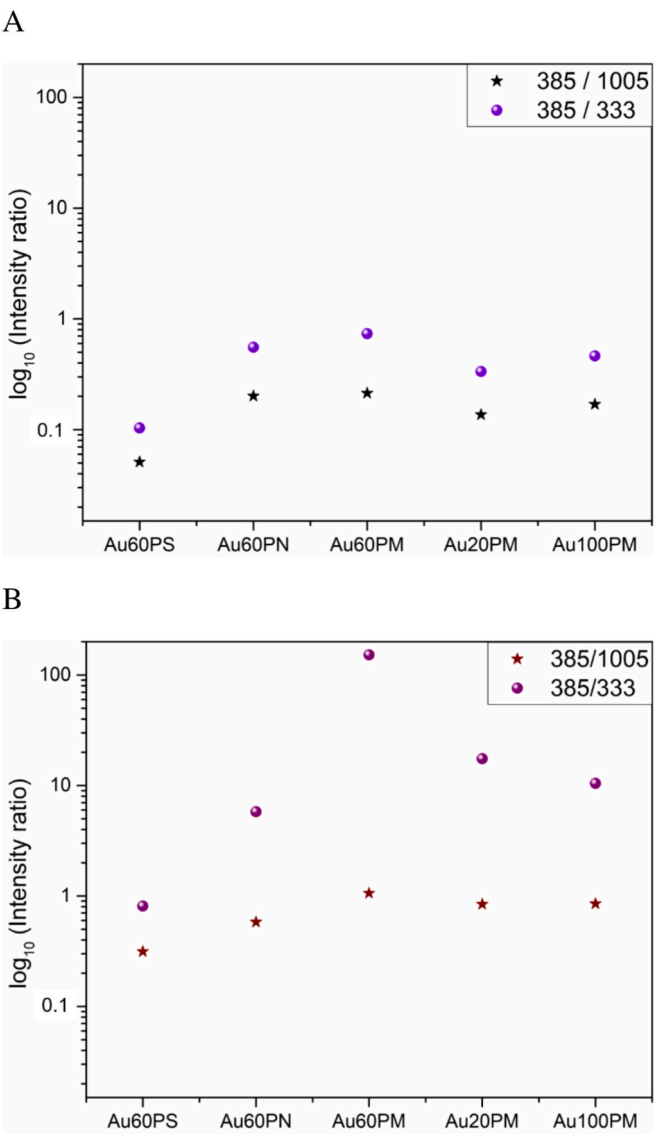

Fig. 5. Mutual intensity ratios of selected SERRS peaks (333, 385, and 1005 cm^{-1}) for (A) freshly prepared and (B) 1-month-aged Au60@polymer nanocomposite-TMPyP6 systems.

3.2. TMPyP interaction with AuNPs of different sizes embedded in pMEO$_2$MA

As demonstrated in the previous section, J-aggregates formation of TMPyP reaches the highest degree on Au60PM nanocomposite. Therefore, we decided to investigate the influence of Au core size while using the same polymeric shell, pMEO$_2$MA. Au core was thus prepared in sizes of approx.20 nm and 100 nm in diameter embedded in pMEO$_2$MA, respectively. The results for Au20PM and Au100PM are listed in Table 1, Table 2, Table SI-1, Table SI-2, Table SI-3, Table SI-4, Table SI-5, Table SI-7 Table SI-8, and shown in Fig. 1, Fig. 5, Figures SI-1, SI-2, SI-5, for the sake of direct comparisons with the Au60PM nanocomposite.

Let's start the discussion from UV–vis measurements again: Soret band is substantially red-shifted (by 6 and 10 nm) in Au@polymer nanocomposite-TMPyP6 systems, whereas the red-shift of the SPE band is negligible (more pronounced in Au100PM-TMPyP6 than in Au20PM-TMPyP6) – Table 1 and Figure SI-2. This corroborates TMPyP J-aggregates formation and corresponds to a thinner polymeric shell around the Au100 core (Table 2), respectively. Furthermore, the addition of TMPyP to AuNP@pMEO$_2$MA core@shell nanocomposites leads to slight changes in zeta potential values (Table SI-2): they become less negative, thus decreasing in absolute values.

Interestingly, fluorescence spectra measured for the Au20PM-TMPyP7 and Au100PM-TMPyP7 systems (Fig. 6) manifested themselves by two separated maxima located at 660 and 720 nm.

It is the same feature as observed in Au60PM-TMPyP7, however, in Au20PM-TMPyP7 and Au100PM-TMPyP7, fluorescence intensity is not quenched to such a large extent as in Au60PM-TMPyP7. Looking at Table 2, polymeric shell thicknesses (derived from hydrodynamic diameter measurements – Table SI-3) are of almost half values at Au20PM and Au100PM than in Au60PM; the smallest polymeric shell encountered in the largest Au core of this study (Au100). Since the polymeric shell is responsible for TMPyP J-aggregates formation in our systems, the thinner the polymeric shell, the lower degree of J-aggregates formation and, consequently, the lower TMPyP fluorescence quenching. Exactly the case observed and shown in Fig. 6: the lowest fluorescence quenching in Au100PM-TMPyP7, followed by Au20PM-TMPyP7.

To validate our hypothesis about the importance of direct molecular interactions while TMPyP J-aggregates formation (and consequent TMPyP fluorescence quenching observation), we measured fluorescence quenching of TMPyP on AuNPs with different ionic envelopes composed of low molecular weight species – Figure SI-10. The experiments (described in detail in Supporting Information) gave direct evidence that TMPyP fluorescence quenching is highly dependent on the character of molecules/ions at the surface of AuNPs, as well as, on the thickness of this envelope surrounding AuNPs as demonstrated in the example of citrate residues – Figure SI-10. However, it should be kept in mind that electrostatic forces dominate in the case of low-molecular-weight species mainly, while other types of noncovalent interactions and steric hindrance can compete in polymeric cases as well.

Last, but not least, SERRS spectra of Au100PM-TMPyP6 and Au20PM-TMPyP6 were measured (at two different temperatures, freshly prepared and/or one month aged) and are shown in Figure SI-11 in the direct comparison to Au60PM-TMPyP6. Consistently with fluorescence, more J-aggregates of TMPyP are generated in Au60PM-TMPyP6 than in the two other cases as demonstrated by increased intensity of J-aggregates SERRS spectral form (markers positioned at 385, 1015 and 1368 cm^{-1}). Considering the excitation laser line applied in SERRS measurements (532 nm), a better resonance with SPE (Table 1) can be assumed in the Au20PM-TMPyP6 system than in the Au100PM-TMPyP6 system (where rather a pre-resonance condition is achieved). On the other hand, Au100PM possesses the highest extinction molar coefficient

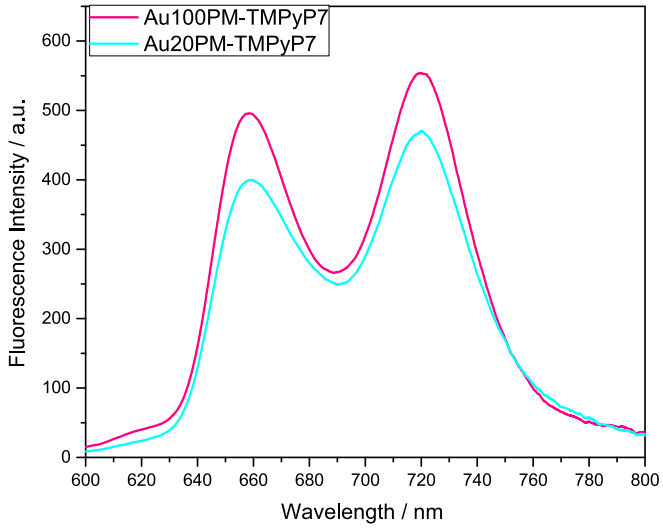

Fig. 6. Fluorescence spectra of Au20PM-TMPyP7 and Au100PM-TMPyP7 systems. Excitation 422 nm.

as calculated in Supporting Information (Table SI-9) based on ICP-MS and extinction experimental data. As a result of these two opposite trends, the intensity of SERRS signals in Au100PM-TMPyP6 and Au20PM-TMPyP6 systems resemble (Figure SI-11).

4. Conclusions

We achieved J-aggregates formation of a tetracationic porphyrin (TMPyP) in its low, therapeutically-relevant concentrations (0.1 and 1 μM) which is unusual. Usually, TMPyP in such low concentrations is incapable of forming aggregates or dimers spontaneously due to the electrostatic repulsion of its positively charged molecules (tetra-cations). However, if interacting with the surface of Au@selected polymer core@shell nanocomposites, TMPyP can be easily detected by SERRS signal in J-aggregates form although TMPyP concentration does not exceed the calculated monolayer TMPyP surface-coverage concentration as demonstrated within this study. Mechanisms of TMPyP aggregation into J-aggregates induced by different polymeric shell types and morphologies of the plasmonic Au core@thermoresponsive polymer nanocomposites are suggested. Owing to the thermo-sensitivity of the polymeric shell surrounding the plasmonic Au core, the SERRS spectroscopic signal of TMPyP J-aggregates even increased at temperatures above 30 °C. The whole procedure of two-step aggregation could be potentially exploited for the detection of cationic species of similar structure to TMPyP in living systems. Moreover, by prolonging the time of TMPyP and Au@smart polymer nanocomposites interaction, further augmentation of the SERRS signal of J-aggregates can be achieved. It should be pointed out that the Au@polymer nanocomposites with J-aggregates of TMPyP are stable over long periods (here demonstrated for 1-month aged samples) and solely reversible nanocomposites aggregation is observed due to the Au core steric protection by polymeric envelope. This is unusual and beneficial simultaneously because many adsorbates are known to cause irreversible plasmonic nanoparticle aggregation. Further spectroscopic data (steady-state fluorescence and UV–vis absorption) supported the J-aggregates formation of TMPyP at the nanocomposite surface. Further experiments are envisaged where the parameters such as thickness and density of polymeric shells will be investigated in conjunction with the selected adsorbate aggregation. The concept of adsorbate aggregation (instead of plasmonic AuNPs aggregation) at the surface of the nanocomposites (selected polymer coated plasmonic AuNPs), i.e., the adsorbate concentrate formation, could be further exploited in biomedical, biological, material, and environmental research dealing with the sensitive and specific detection of low concentrations of species (e.g., biologically active molecules, drugs, and/or pollutants of emerging concerns).

Credit authorship contribution statement

KS: Conceptualization, Resources, Investigation, Methodology, Funding acquisition, Data analysis and interpretation, Writing and editing original draft, Original draft - review & editing. NG: Conseptualization, Investigation, Methodology, Original draft - review & editing, Funding acquisition. MGS: Investigation. JK: Investigation, Formal spectral analysis, Original draft - review & editing.

Declaration of competing interest

The authors declare that they have no known competing financial interests or personal relationships that could have appeared to influence the work reported in this paper.

Acknowledgement

Financial support by the Czech Science Foundation (project no. 25-15590S) is gratefully acknowledged. Grant MAT2014-57429-R supported by Spanish MINECO and TED2021-129959B-C22, funded by MCIN/AEI/10.13039/501100011033 and 'European Union Next Generation EU/PRTR' are acknowledged. The authors acknowledge the assistance provided by the Research Infrastructure NanoEnviCz, supported by the Ministry of Education, Youth and Sports of the Czech Republic under Project No. LM2018124. Jana Stráská and Tomáš Pluháček are thanked for the TEM/EDS measurements and ICP-MS analysis, respectively. Radek Ostruszka and Veronika Svačinová are acknowledged for additional DLS measurements and PSD determination, respectively.

Appendix A. Supplementary data

Supplementary data to this article can be found online at https://doi.org/10.1016/j.saa.2025.127158.

Data availability

The raw/processed data required to reproduce these findings can be sent on demand from the corresponding author and/or from the repository at Dept. of Experimental Physics, Faculty of Science, Palacký University Olomouc (administered by M. Vůjtek: milan.vujtek@upol.cz).

References

[1] M. Moskovits, Surface-enhanced spectroscopy, Rev. Mod. Phys. 57 (1985) 783–826, https://doi.org/10.1016/B0-12-369397-7/00532-X.
[2] S.E. Seo, E. Ryu, J. Kim, C.J. Shin, O.S. Kwon, Fluorophore-encapsulated nanobeads for on-site, rapid, and sensitive lateral flow assay, Sensors Actuators B Chem. 381 (2023) 133364, https://doi.org/10.1016/j.snb.2023.133364.
[3] Y.H. Huang, H. Wei, P.J. Santiago, W.J. Thrift, R. Ragan, S. Jiang, Sensing antibiotics in wastewater using surface-enhanced Raman scattering, Environ. Sci. Technol. 57 (2023) 4880–4891, https://doi.org/10.1021/acs.est.3c00027.
[4] S. Sadik, S. Columbus, S. Bhattacharjee, S.S. Nazeer, K. Ramachandran, K. Daoudi, H. Alawadhi, M. Gaidi, A. Shanableh, Smart optical sensing of multiple antibiotic residues from wastewater effluents with ensured specificity using SERS assisted with multivariate analysis, Environ. Pollut. 343 (2024) 123229, https://doi.org/10.1016/j.envpol.2023.123229.
[5] W.K. Son, Y.S. Choi, Y.W. Han, D.W. Shin, K. Min, J. Shin, M.J. Lee, H. Son, D. H. Jeong, S.Y. Kwak, In vivo surface-enhanced Raman scattering nanosensor for the real-time monitoring of multiple stress signalling molecules in plants, Nat. Nanotechnol. 18 (2023) 205–216, https://doi.org/10.1038/s41565-022-01274-2.
[6] D. Song, R. Yang, F. Long, A. Zhu, Applications of magnetic nanoparticles in surface-enhanced Raman scattering (SERS) detection of environmental pollutants, J. Environ. Sci. (China) 80 (2019) 14–34, https://doi.org/10.1016/j.jes.2018.07.004.
[7] A.P. Francisco, D. Botequim, D.M.F. Prazeres, V.V. Serra, S.M.B. Costa, C.A.T. Laia, P.M.R. Paulo, Extreme enhancement of single-molecule fluorescence from porphyrins induced by gold Nanodimer antennas, J. Phys. Chem. Lett. 10 (2019) 1542–1549, https://doi.org/10.1021/acs.jpclett.9b00373.
[8] B. Vlčková, M. Moskovits, I. Pavel, K. Šišková, M. Sládková, M. Šlouf, Single-molecule surface-enhanced Raman spectroscopy from a molecularly-bridged silver nanoparticle dimer, Chem. Phys. Lett. 455 (2008) 131–134, https://doi.org/10.1016/j.cplett.2008.02.078.
[9] M. Pacaud, K. Hervé-Aubert, M. Soucé, A.A. Makki, F. Bonnier, A. Fahmi, A. Feofanov, I. Chourpa, One-step synthesis of gold nanoflowers of tunable size and absorption wavelength in the red & deep red range for SERS spectroscopy, Spectrochim, Acta - Part A Mol. Biomol. Spectrosc. 225 (2020) 117502, https://doi.org/10.1016/j.saa.2019.117502.
[10] I. Šloufová, K. Šišková, B. Vlčková, J. Štěpánek, SERS-activating effect of chlorides on borate-stabilized silver nanoparticles: formation of new reduced adsorption sites and induced nanoparticle fusion, Phys. Chem. Chem. Phys. 10 (2008) 2233–2242, https://doi.org/10.1039/b718178g.
[11] V. Sutrová, I. Šloufová, M. Nevoralová, B. Vlčková, SERS microRaman spectral probing of adsorbate-containing, liquid-overlayed nanosponge ag aggregates assembled from fractal aggregates, J. Raman Spectrosc. 46 (2015) 559–565, https://doi.org/10.1002/jrs.4690.
[12] V.N. Zozulya, O.A. Ryazanova, I.M. Voloshin, A.Yu. Glamazda, V.A. Karachevtsev, Spectroscopic detection of tetracationic porphyrin H-aggregation on polyanionic matrix of inorganic polyphosphate, J. Fluoresc. 20 (2010) 695–702, https://doi.org/10.1007/s10895-010-0609-1.
[13] V.K. Sharma, K.M. Siskova, R. Zboril, J.L. Gardea-Torresdey, Organic-coated silver nanoparticles in biological and environmental conditions: fate, stability and toxicity, Adv. Colloid Interf. Sci. 204 (2014) 15–34, https://doi.org/10.1016/j.cis.2013.12.002.
[14] Z. Abousalman-Rezvani, H. Roghani-Mamaqani, H. Riazi, O. Abousalman-Rezvani, Water treatment using stimuli-responsive polymers, Polym. Chem. 13 (2022) 5940–5964, https://doi.org/10.1039/d2py00992g.

[15] O. Guselnikova, P. Postnikov, Y. Kalachyova, Z. Kolska, M. Libansky, J. Zima, V. Svorcik, O. Lyutakov, Large-scale ultrasensitive highly reproducible and reusable smart SERS platform based.Pdf, ChemNanoMat 3 (2017) 135–144.
[16] B. Hu, D.W. Sun, H. Pu, Q. Wei, A dynamically optical and highly stable pNIPAM @ Au NRs nanohybrid substrate for sensitive SERS detection of malachite green in fish fillet, Talanta 218 (2020) 121188, https://doi.org/10.1016/j.talanta.2020.121188.
[17] N. Guarrotxena, I. Quijada-Garrido, Optical and swelling stimuli-response of functional hybrid Nanogels: feasible route to achieve tunable smart Core@Shell Plasmonic@polymer nanomaterials, Chem. Mater. 28 (2016) 1402–1412, https://doi.org/10.1021/acs.chemmater.5b04517.
[18] M. Liras, O. García, N. Guarrotxena, M. Palacios-Cuesta, I. Quijada-Garrido, Versatile thiolated thermosensitive polymers synthesized by ATRP of MEO2MA and AcSEMA, a new methacrylic monomer with a protected thiol group, Polym. Chem. 4 (2013) 5751–5759, https://doi.org/10.1039/c3py00773a.
[19] N. Guarrotxena, O. García, I. Quijada-Garrido, Synthesis of Au@polymer nanohybrids with transited core-shell morphology from concentric to eccentric emoji-N or Janus nanoparticles, Sci. Rep. 8 (2018) 1–9, https://doi.org/10.1038/s41598-018-24078-8.
[20] A. Soto-Quintero, N. Guarrotxena, O. García, I. Quijada-Garrido, Curcumin to promote the synthesis of silver NPs and their self-assembly with a Thermoresponsive polymer in Core-Shell Nanohybrids, Sci. Rep. 9 (2019) 1–14, https://doi.org/10.1038/s41598-019-54752-4.
[21] N. Guarrotxena, L. Garrido, I. Quijada-Garrido, Design of Nanostructured Surfaces Based on metal NP precipitation strategy and their catalytic application, Adv. Mater. Interfaces 5 (2018) 1–9, https://doi.org/10.1002/admi.201801374.
[22] A. Lapresta-Fernández, J.M. García-García, R. París, R. Huertas-Roa, A. Salinas-Castillo, S.A. De La Llana, J.F. Huertas-Pérez, N. Guarrotxena, L.F. Capitán-Vallvey, I. Quijada-Garrido, Thermoresponsive gold polymer nanohybrids with a tunable cross-linked meo 2 ma polymer shell, Part. Part. Syst. Charact. 31 (2014) 1183–1191, https://doi.org/10.1002/ppsc.201400078.
[23] V. Cenklová, Photodynamic therapy with TMPyP – Porphyrine induces mitotic catastrophe and microtubule disorganization in HeLa and G361 cells, a comprehensive view of the action of the photosensitizer, J. Photochem. Photobiol. B Biol. 173 (2017) 522–537, https://doi.org/10.1016/j.jphotobiol.2017.06.029.
[24] J. Wang, Z. Zhang, S. Zha, Y. Zhu, P. Wu, B. Ehrenberg, J.Y. Chen, Carbon nanodots featuring efficient FRET for two-photon photodynamic cancer therapy with a low fs laser power density, Biomaterials 35 (2014) 9372–9381, https://doi.org/10.1016/j.biomaterials.2014.07.063.
[25] D.C. Ferreira, C.S. Monteiro, C.R. Chaves, G.A.M. Sáfar, R.L. Moreira, M.V. B. Pinheiro, D.C.S. Martins, L.O. Ladeira, K. Krambrock, Hybrid systems based on gold nanostructures and porphyrins as promising photosensitizers for photodynamic therapy, Colloids Surf. B: Biointerfaces 150 (2017) 297–307, https://doi.org/10.1016/j.colsurfb.2016.10.042.
[26] R.W.Y. Sun, C.K.L. Li, D.L. Ma, J.J. Yan, C.N. Lok, C.H. Leung, N. Zhu, C.M. Che, Stable anticancer gold(III)-porphyrin complexes: effects of porphyrin structure, Chem. - A Eur. J. 16 (2010) 3097–3113, https://doi.org/10.1002/chem.200902741.
[27] F.J. Vergeldt, R.B.M. Koehorst, A. Van Hoek, T.J. Schaafsma, Intramolecular interactions in the ground and excited state of tetrakis(N-methylpyridyl) porphyrins, J. Phys. Chem. 99 (1995) 4397–4405, https://doi.org/10.1021/j100013a007.
[28] K. Šišková, B. Vlčková, P. Mojzeš, Spectral detection of J-aggregates of cationic porphyrin and investigation of conditions of their formation, J. Mol. Struct. 744–747 (2005) 265–272, https://doi.org/10.1016/j.molstruc.2004.10.047.
[29] K. Siskova, B. Vlckova, P.Y. Turpin, A. Thorel, A. Grosjean, Porphyrins as SERRS spectral probes of chemically functionalized Ag nanoparticles, Vib. Spectrosc. 48 (2008) 44–52, https://doi.org/10.1016/j.vibspec.2008.04.006.
[30] K. Šišková, B. Vlčková, P.Y. Turpin, A. Thorel, M. Procházka, Laser ablation of silver in aqueous solutions of organic species: probing ag nanoparticle-adsorbate systems evolution by surface-enhanced raman and surface plasmon extinction spectra, J. Phys. Chem. C 115 (2011) 5404–5412, https://doi.org/10.1021/jp110907d.
[31] K. Šišková, O. Bečička, V. Mašek, K. Šafářová, R. Zbořil, Spacer-free SERRS spectra of unperturbed porphyrin detected at 100 fM concentration in Ag hydrosols prepared by modified Tollens method, J. Raman Spectrosc. 43 (2012) 689–691, https://doi.org/10.1002/jrs.3098.
[32] I. Vilímová, K. Šišková, Distinctly different morphologies of bimetallic au-ag nanostructures and their application in submicromolar Sers-detection of free base porphyrin, Nanomaterials 11 (2021), https://doi.org/10.3390/nano11092185.
[33] N.C. Maiti, S. Mazumdar, N. Periasamy, J- and H-aggregates of porphyrin - surfactant complexes: time-resolved fluorescence and other spectroscopic studies, J. Phys. Chem. B 102 (1998) 1528–1538, https://doi.org/10.1021/jp9723372.
[34] J. Dolanský, P. Henke, P. Kubát, A. Fraix, S. Sortino, J. Mosinger, Polystyrene nanofiber materials for visible-light-driven dual antibacterial action via simultaneous Photogeneration of NO and O2(1δg), ACS Appl. Mater. Interfaces 7 (2015) 22980–22989, https://doi.org/10.1021/acsami.5b06233.
[35] M. Kossakowska-Zwierucho, G. Szewczyk, T. Sarna, J. Nakonieczna, Farnesol potentiates photodynamic inactivation of *Staphylococcus aureus* with the use of red light-activated porphyrin TMPyP, J. Photochem. Photobiol. B Biol. 206 (2020) 111863, https://doi.org/10.1016/j.jphotobiol.2020.111863.
[36] A.M. Santoro, M.C. Lo Giudice, A. D'Urso, R. Lauceri, R. Purrello, D. Milardi, Cationic porphyrins are reversible proteasome inhibitors, J. Am. Chem. Soc. 134 (2012) 10451–10457, https://doi.org/10.1021/ja300781u.
[37] R.T. Wheelhouse, D. Sun, H. Han, F.X. Han, L.H. Hurley, Cationic porphyrins as telomerase inhibitors: the interaction of tetra- (N-methyl-4-pyridyl)porphine with quadruplex DNA [1], J. Am. Chem. Soc. 120 (1998) 3261–3262, https://doi.org/10.1021/ja973792e.
[38] G. Sallam, S.Y. Shaban, A. Nassar, M.E. El-Khouly, Water soluble porphyrin as optical sensor for the toxic heavy metal ions in an aqueous medium, Spectrochim, Acta - Part A Mol. Biomol. Spectrosc. 241 (2020) 118609, https://doi.org/10.1016/j.saa.2020.118609.
[39] R. Ostruszka, D. Půlpánová, T. Pluháček, O. Tomanec, P. Novák, D. Jirák, K. Šišková, Facile one-pot green synthesis of magneto-luminescent bimetallic nanocomposites with potential as dual imaging agent, Nanomaterials 13 (2023) 1027, https://doi.org/10.3390/nano13061027.
[40] N. Blom, J. Odo, K. Nakamoto, D.P. Strommen, Resonance Raman studies of metal tetrakis(4-N-methylpyridyl)porphine: band assignments, structure-sensitive bands, and species equilibria, J. Phys. Chem. 90 (1986) 2847–2852, https://doi.org/10.1021/j100404a015.
[41] M. Procházka, P.Y. Turpin, J. Štěpánek, B. Vlčková, SERRS of free base porphyrin in laser-ablated colloids: evidence for three different spectral porphyrin forms, J. Raman Spectrosc. 33 (2002) 758–760, https://doi.org/10.1002/jrs.910.
[42] N. Hajduková-Šmídová, M. Procházka, M. Osada, SE(R)RS excitation profile of free-base 5,10,15,20-tetrakis(1-methyl-4- pyridyl) porphyrin on immobilized gold nanoparticles, Vib. Spectrosc. 62 (2012) 115–120, https://doi.org/10.1016/j.vibspec.2012.04.007.
[43] R. Pelton, Poly(N-isopropylacrylamide) (PNIPAM) is never hydrophobic, J. Colloid Interface Sci. 348 (2010) 673–674, https://doi.org/10.1016/j.jcis.2010.05.034.
[44] E. Dalgakiran, H. Tatlipinar, Atomistic insights on the LCST behavior of PMEO2MA in water by molecular dynamics simulations, J. Polym. Sci. Part B Polym. Phys. 56 (2018) 429–441, https://doi.org/10.1002/polb.24555.
[45] S. Zhao, Y. Song, L. Xu, H. Hu, J. Wang, F. Huang, L. Shi, Self-assembly nanochaperone with tunable hydrophilic–hydrophobic surface for controlled protein refolding, Macromol. Biosci. 23 (2023) 1–8, https://doi.org/10.1002/mabi.202300205.
[46] J.H.L. Ngai, J.K.W. Ho, R.K.H. Chan, S.H. Cheung, L.M. Leung, S.K. So, Growth, characterization, and thin film transistor application of CH3NH3PbI3 perovskite on polymeric gate dielectric layers, RSC Adv. 7 (2017) 49353–49360, https://doi.org/10.1039/c7ra08699g.